Letters

Development of an Ultrafast Hybrid Circuit Breaker With a Novel Arc-Enhanced Lightweight Mechanical Switch for Low-Voltage DC Applications

Tianpei Shan, Yifei Wu, Yi Wu, Heming Zhu, Yu Xiao, and Mingzhe Rong

***Abstract*—The hybrid dc circuit breaker (HCB) is crucial for clearing faults and ensuring a reliable power supply in dc grids. However, the fault current can rise rapidly in the low-voltage dc systems, and existing traditional HCB solutions cannot meet the demands of speed and size due to the structure design of the fast mechanical switch and additional assisted commutation devices. In this letter, a novel arc-enhanced lightweight ultrafast mechanical switch is proposed for low-voltage HCBs. Compared to traditional fast mechanical switches designed for HCBs, the proposed ultrafast mechanical switch offers an extremely fast inherent opening time and current interruption time by eliminating the unnecessary arc extinguishing chamber and applying an innovative dual-stage motion design. Meanwhile, the structure of double-point contact enhances the arc voltage, enabling faster current commutation to the power electronic switch without any bulky auxiliary device. After parameter design and optimization, a compact 750-V HCB prototype based on the novel ultrafast mechanical switch is built to verify the feasibility. The prototype has an inherent opening time of 70 μs and can interrupt a 26 kA current within 400 μs.**

***Index Terms*—Current commutation, fast mechanical switch (MS), hybrid circuit breaker (HCB).**

I. Introduction

THE low-voltage dc distribution system adequately supports the integration of distributed renewable energy sources, energy storage devices, and various complex loads, providing flexible, efficient, and reliable power services for users [1], [2]. However, to achieve dc interconnected grids, it is essential to incorporate a high proportion of power electronic energy conversion devices and large-scale energy storage components, which leads to the unique weak-damping fault characteristic of the dc distribution system [3]. Compared to the medium-voltage dc transmission system, the low-voltage distribution system also cannot install enough reactors to limit the dc fault currents, and the rate of fault current rise (several tens of amperes per microsecond) is significantly higher under the typical system configuration [4].

Considering the absence of a current zero-crossing point in dc power systems, dc circuit breakers are crucial for achieving rapid protection against dc faults [5]. In engineering, air circuit breakers (ACB) and solid-state circuit breakers (SSCB) are the most commonly used in low-voltage dc current interruption applications. Traditional ACBs can break large fault currents and have low conduction losses, but they also exhibit inherent drawbacks, such as slow operating speed, short service life, and severe arc flashing [6], [7]. SSCBs use power electronic devices to conduct load current, enabling extremely fast fault protection. However, the relatively high conduction losses and the need for cooling devices limit their applicability in high-capacity current interruption scenarios [8].

Combining the advantages of fast mechanical switch (MS) and power electronic switch (PES), the hybrid circuit breakers (HCB) not only have sufficient fault current breaking capacity but also feature flexible reclosing function and low conduction losses. Currently, the technical solutions for the HCB are well established, with many prototypes and projects demonstrating their feasibility in the medium- and high-voltage engineering [9], [10]. The traditional HCB solution and the typical structure of the used fast MS are shown in Fig. 1. Existing fast MS used for HCBs are commonly based on vacuum arc extinguishing chambers and the operational mechanism of the Thomson coil actuator. Although existing vacuum fast MS have addressed the key issue of restoring insulation performance to withstand the overvoltage of current interruption, the contact's opening separation speed remains nonideal. Thus, the inherent opening time and the current interruption time of existing HCB solutions are greater than 1 ms and 2 ms, respectively [11], [12]. Besides, most HCB solutions have included a bulky auxiliary commutation device (even a water-cooling system), because a single vacuum arc voltage is insufficient for the fast current transfer from the MS to the PES [13], [14]. Overall, the fast MS based on a traditional structure limits the expansion of HCBs in low-voltage applications due to constraints in speed and size.

To achieve faster fault protection in dc distribution systems, this letter proposes a novel arc-enhanced lightweight ultrafast MS, specifically designed for low-voltage HCBs. First, based

Received 1 October 2025; revised 5 November 2025; accepted 24 November 2025. Date of publication 2 December 2025; date of current version 19 January 2026. This work was supported in part by the National Natural Science Foundation of China under Grant 52025074, Grant 52377158, and Grant U22B20121, and in part by the Independent Research Project of the State Key Laboratory of Electrical Insulation and Power Equipment of China under Grant EIPE23113. *(Corresponding author: Yifei Wu, Yi Wu.)*

The authors are with the State Key Laboratory of Electrical Insulation and Power Equipment, Xi'an Jiaotong University, Xi'an 710049, China (e-mail: shantianpei@stu.xjtu.edu.cn; yifei208@xjtu.edu.cn; wuyic51@xjtu.edu.cn; 3123304055@stu.xjtu.edu.cn; y.xiao@xjtu.edu.cn; mzrong@mail.xjtu.edu.cn).

Color versions of one or more figures in this article are available at https://doi.org/10.1109/TPEL.2025.3639479.

Digital Object Identifier 10.1109/TPEL.2025.3639479

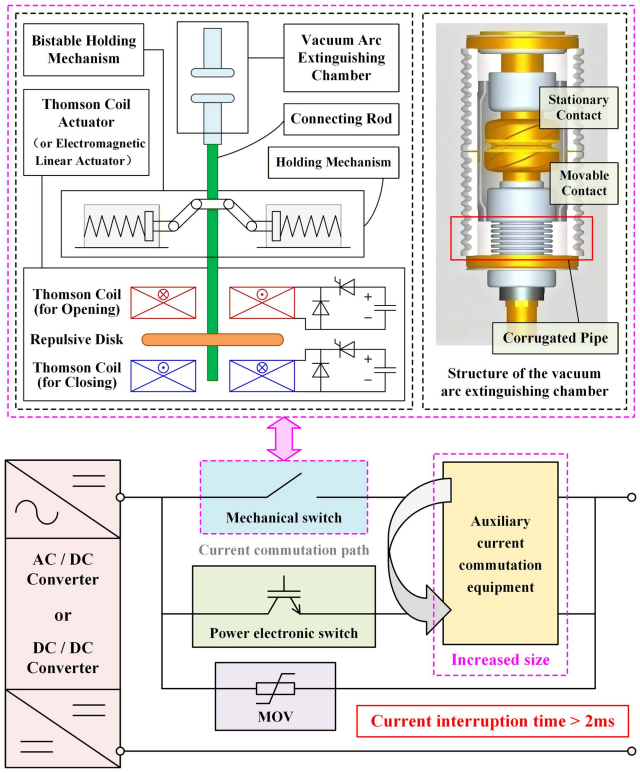

Fig. 1. Traditional HCB solution and the typical fast MS structure [9], [10].

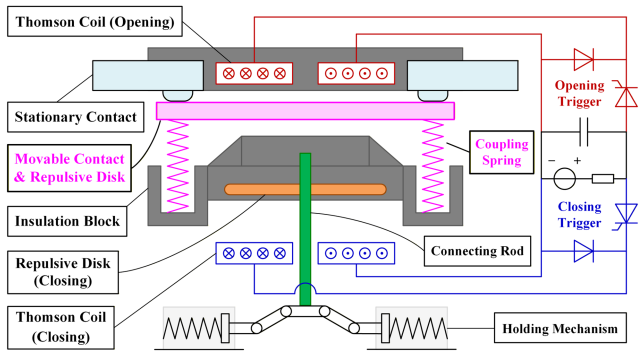

Fig. 2. Structure of the novel lightweight ultrafast MS.

on an HCB dielectric recovery condition with zero voltage and current for the MS, an unnecessary arc extinguishing chamber is eliminated to reduce the motion resistance for the movable contact and accelerate its opening separation speed. Second, a novel design concept of the dual-stage lightweight motion is proposed to accelerate the movable contact's separation speed before the current interruption's moment by reducing both the number and mass of the moving components. Third, the dual-point contact structure is employed to enhance the arc voltage, ensuring the current can rapidly commutate from the MS to the PES. Thus, the proposed ultrafast MS can offer an extremely fast inherent opening time of 70 μs, and achieve a contact gap of more than 2 mm within 400 μs after receiving the opening command. Through a discussion of the operation processes and parameter design, the feasibility of the proposed ultrafast MS and the HCB solution based on it has been validated by the test results from a 750-V HCB prototype, which has successfully interrupted currents of 12 and 26 kA within 400 μs.

II. Proposed Novel Ultrafast Mechanical Switch

A. Structure Solution

As shown in Fig. 2, the novel lightweight ultrafast MS consists of two parts: the mechanical structure and the drive circuit. The mechanical structure includes Thomson coils (for opening and closing), the stationary contact, the novel movable contact integrating the function of a metal repulsive disk, the coupling springs designed for a dual-stage motion, the insulation block, the connecting rod, the metal repulsive disk for closing, and the holding mechanism. The drive circuit includes a low-power dc charging device (with small size and cheap cost), precharging capacitors, triggered thyristors, and freewheeling diodes.

Based on the electromagnetic repulsive force principle with the Thomson coil actuator, a pulse current will be activated in the Thomson coil by the feed from the precharged capacitors. Due to the opposing directions of the magnetic field generated by the pulse current of the Thomson coil and the magnetic field generated from the induced eddy currents in the metal repulsive disk, a strong mutual repulsive Lorentz force is generated. As shown in Fig. 1, the traditional fast MS structure features three main points: the vacuum arc extinguishing chamber, the overall motion design where the metal repulsive disk pulls the movable contact, connecting rod, and holding mechanism together, and the single-point contact structure. For the proposed lightweight ultrafast MS, the significant innovations can be summarized in the following three corresponding key points.

1) Due to a comfortable dielectric recovery condition of the HCB (with both zero voltage and current) and the overvoltage level clamped by the MOV to below 2 p.u. of the rated voltage, the unnecessary arc extinguishing chamber has been eliminated, reducing the opening motion resistance of the movable contact and improving its opening separation speed.
2) A novel operational structure of dual-stage motion has been designed. In the design, the opening separation process of the proposed ultrafast MS can be divided into the first stage of rapid lightweight motion and the second stage of decelerated overall motion. To achieve ultrafast motion in the first stage, the proposed ultrafast MS has greatly reduced the equivalent motion resistance of the moving components by retaining only the movable contact and coupling spring during this stage. By setting the coupling spring to get rid of the motion resistance from the excess burden (such as an extra metal repulsive disk, a connecting rod, and a holding mechanism), and combining the movable contact with the opening repulsive disk into a single unit, the equivalent mass of moving components is minimized. Therefore, the lightweight motion mass achieves an ultrafast separation speed, which further helps reduce both the inherent opening time and the current interruption time of HCBs.

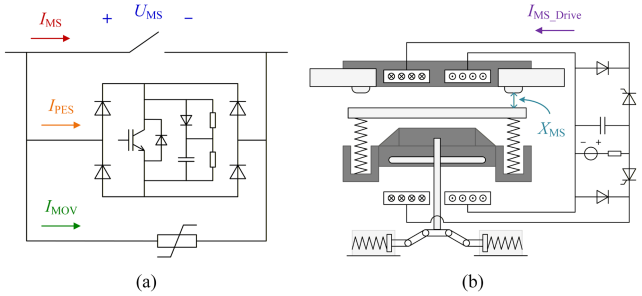

Fig. 3. Variable names and related reference directions. (a) Variable names of the HCB. (b) Variable names of the ultrafast MS.

3) Two sets of contacts have been designed in the proposed ultrafast MS, effectively doubling the arc voltage compared to the single-point contact structure. By the natural commutation characteristics of the air arc, the fault current can be quickly transferred from the MS to the PES without the need for any bulky auxiliary equipment.

Besides, for the ultrafast MS, the opening Thomson coil is relocated to the top position, approaching the movable contact.

B. Operation Process

To improve readability and maintain consistency throughout this letter, the variable names and the reference directions for the current, voltage, and distance are shown in Fig. 3. The key variables of the ultrafast MS used in HCB are illustrated in Fig. 3(b). $I_{\mathrm{MS\_Drive}}$ means the pulse current flowing in the Thomson coil for opening, which is generated by the thyristor discharging and the diode freewheeling, and X_{MS} denotes the gap distance between the movable contact and the stationary contact.

As shown in Figs. 4 and 5, the operation processes of the ultrafast MS and the related ultrafast HCB solution based on it are illustrated in detail. For any allowed *di/dt* of fault current, the operation process of the ultrafast HCB is always the same after getting the opening command from the protection device.

Before t_0: A short-circuit fault current with a rapid rise rate occurs and flows through the ultrafast MS.

t_0-t_1: At $t = t_0$, the fault is detected, and the MS receives the opening command. The precharging capacitors discharge to the opening Thomson coil through the opening triggered thyristor, forming a pulsed current. With a pulsed current magnetic field, eddy currents are generated inside the movable contact, causing an electromagnetic repulsive force for separating. However, due to the initial holding force of the coupling spring, the movable contact remains engaged with the stationary contact during this stage, as shown in Fig. 4(a).

t_1-t_2: At $t = t_1$, after the inherent opening time from t_0-t_1, the movable contact actually separates from the stationary contact, and the doubled arc voltage is developed between two sets of contacts. Under the enhanced arc voltage, the current promptly transfers to the PES from the MS, as shown in Fig. 4(b).

t_2-t_3: At $t = t_2$, the current has been completely transferred from the MS to the PES. The MS begins to recover its insulation performance under the PES low conduction voltage, while the movable contact continues to separate away from the stationary contact, as shown in Fig. 4(c). Anticipatorily, when the movable contact strikes the insulation block (this moment is designed before t_3), the insulation distance will be sufficient to withstand the following turn-OFF overvoltage, as shown in Fig. 4(d). It is worth noting that when the movable contact hits the insulation block, it will slightly stagnate and continue to move downward by the mode of decelerated overall motion.

t_3-t_4: At $t = t_3$, the PES turns OFF the current, redirecting it to the MOV, which clamps the overvoltage to nearly the residual voltage (U_{res}) and dissipates the massive inductive energy stored in the dc system. Meanwhile, the movable contact continues to move downward along with the insulation block as one whole unit until the bistable holding mechanism at the bottom passes the inflection point, as shown in Fig. 4(e).

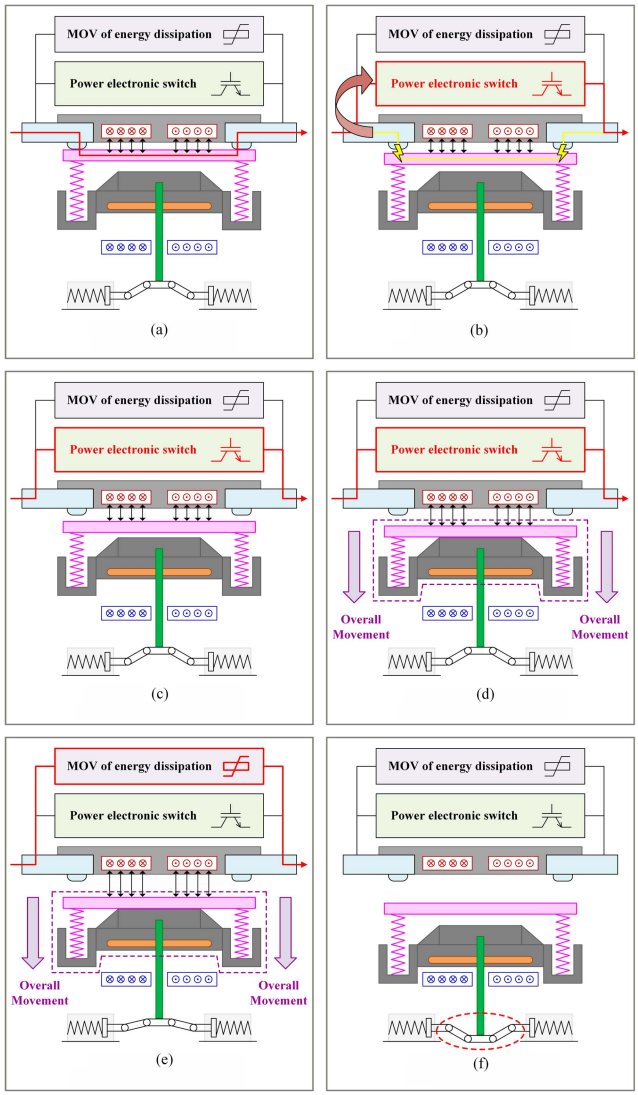

Fig. 4. Operating process of the proposed ultrafast MS. (a) Opening mode I (t_0-t_1: current in MS). (b) Opening mode I (t_1-t_2: current commutation). (c) Opening mode I (t_2-t_3: dielectric recovery). (d) Opening mode II (t_2-t_3: dielectric recovery). (e) Opening mode II (t_3-t_4: current interruption). (f) Opening mode II (after t_4: holding stable).

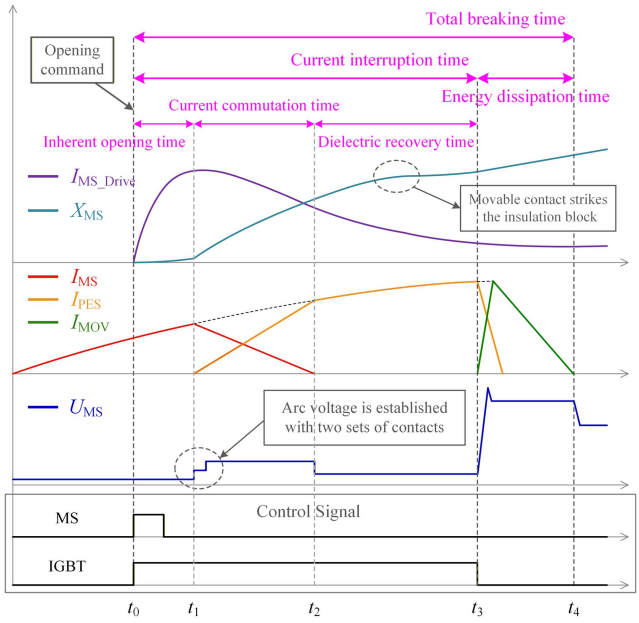

Fig. 5. Operating process of the HCB based on the proposed ultrafast MS.

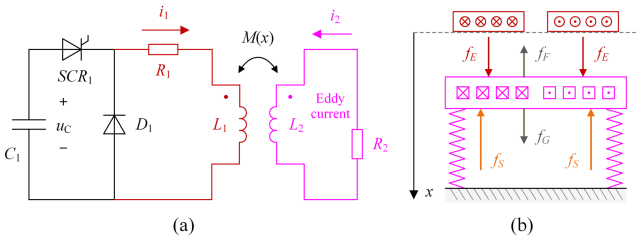

Fig. 6. Operation principles of novel electromagnetic repulsive structure. (a) The coupling model of electromagnetism. (b) The coupling model of force and motion.

After t_4: the HCB's voltage returns to the rated voltage, and the bistable holding mechanism maintains the opening position, as shown in Fig. 4(f).

III. Principle Analysis and Parameter Design

For the proposed ultrafast MS, the fundamental analysis of its operating principle is conducted using electromagnetic field theory and classical mechanics. The electromagnetic coupling analysis of the MS's opening operation can be described using the circuit model based on the mutual inductance affected by displacement, as illustrated in Fig. 6(a) and (1). The coupling principle of force and motion can be derived from the law of energy conservation and the formulas of classical mechanics, as shown in Fig. 6(b) and (2).

In Fig. 6 and the following, L_1 and L_2, i_1 and i_2, and R_1 and R_2 denote the self-inductance, current, and equivalent resistance of the opening Thomson coil and the movable contact (also metal repulsive disk), respectively. M denotes the mutual inductance between the movable contact and the opening Thomson coil. u_C denotes the voltage of the precharging capacitor. U_0 denotes the initial precharged voltage. x denotes the distance between the movable contact and the opening Thomson coil. x_0 denotes the initial distance. f_E, f_S, f_F, and f_G represent the electromagnetic repulsive force, the holding force of the coupling springs, the frictional force, and the gravity, respectively. f_A means the total force obtained by the movable contact, and F_0 means the initial tension force of the coupling spring in the uncompressed state. Compared to the f_E and f_S, the f_F and f_G seem so slight that they could be neglected during parameter design and simulation.

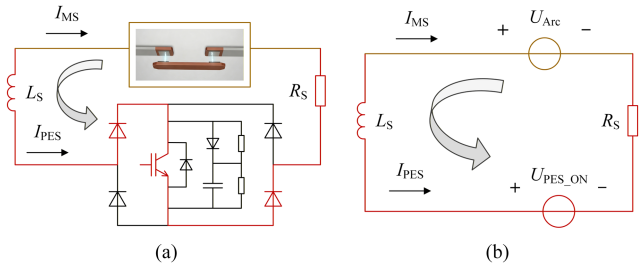

Fig. 7. Circuit model of natural current commutation. (a) Commutation process. (b) Simplified equivalent circuit of the commutation process.

$$\begin{cases} u_C(t) = L_1 \frac{di_1(t)}{dt} + i_1(t) R_1 + M(x) \frac{di_2(t)}{dt} \\ 0 = L_2 \frac{di_2(t)}{dt} + i_2(t) R_2 + M(x) \frac{di_1(t)}{dt} \\ u_C(t) = U_0 - \frac{1}{C_1} \int_{t_0}^{t} i_1(t) \cdot dt \end{cases} \tag{1}$$

$$\begin{aligned} f_A &= ma = m\frac{d^2x}{dt^2} = f_E + f_G - f_F - f_S \\ &\approx f_E - f_S = -\frac{i_1 i_2 dM(x)}{dx} - [k_0(x - x_0) + F_0]. \end{aligned} \tag{2}$$

By simulating the combined mechanical motion and electromagnetism, the displacement trajectory of the movable contact during the opening process can be calculated. Significantly, in practical design, once the movable contact strikes the insulation block, the acceleration trend will be dampened. Therefore, after this moment, the clearance between the movable contact and the stationary contact is sufficient to withstand the PES's turn-OFF overvoltage, as shown in (3). X_{Safe} means the safe distance of the contact gap that can withstand the PES turn-OFF overvoltage.

$$x(t_3) \geq X_{\text{Safe}}. \tag{3}$$

Due to the fast inherent opening time of the novel ultrafast MS, once the movable separates from the stationary contact, the current will rapidly transfer from the MS to the PES due to the arc voltage based on the double near-cathode voltage, as shown in Fig. 7 and (4). In (4), L_S and R_S respectively denote the stray inductance and resistance of the transfer branch of PES, $u_{\text{PES\_ON}}$ denotes the conducting voltage drop of the PES.

The air arc voltage consists of the near-cathode voltage, arc column voltage, and near-anode voltage. With a small contact gap, both the arc column voltage and near-anode voltage are nearly zero. Thus, the total arc voltage is approximately equal to the near-cathode voltage. Besides, the near-cathode voltage is independent of the contact gap and is considered a constant that depends on the contact material.

$$U_{\text{Arc}} = 2 \cdot U_{\text{Near-Cathode}} = L_S \frac{di_{\text{PES}}}{dt} + R_S i_{\text{PES}} + u_{\text{PES\_ON}}. \tag{4}$$

The selection principles for the PES and MOV, which could refer to the existing HCB solutions, are briefly discussed in this letter [15], [16]. As illustrated in (5), the desaturation current

($I_{\mathrm{IGBT\_max}}$) of the IGBT should be greater than the maximum current the IGBT needs to turn OFF ($I_{\mathrm{turn\text{-}OFF\_max}}$). In (5), V_{GE} means the IGBT gate drive voltage, α and γ are the constants related to the IGBT type. As shown in (6), the temperature rise of the IGBT (ΔT) should not exceed the specified limit after the fault current has conducted during the current commutation time and the dielectric recovery time. In (6), P_{IGBT} represents the IGBT power, and Z_{th} means the IGBT thermal resistance. As shown in (7), the transient power (P_{OFF}) and turn-OFF energy (E_{OFF}) during the IGBT interrupt current could not exceed the permissible values. As shown in (8), the energy dissipated by the MOV (E_{MOV}) should not exceed the allowed value.

$$I_{\mathrm{IGBT\_max}} = \alpha(V_{\mathrm{GE}} - V_{\mathrm{T}})^{\gamma} > I_{\mathrm{turn-OFF\_max}} \tag{5}$$

$$\Delta T = P_{\mathrm{IGBT}}(t) * \frac{dZ_{\mathrm{th}}(t)}{dt} = \int_{t_1}^{t_3} P_{\mathrm{IGBT}}(x) \cdot \frac{dZ_{\mathrm{th}}(t-x)}{dt} dx < \Delta T_{\max} \tag{6}$$

$$\begin{cases} P_{\mathrm{OFF}}(t) = U_{\mathrm{IGBT}}(t) \cdot I_{\mathrm{IGBT}}(t) \le P_{\mathrm{OFF\_max}} \\ E_{\mathrm{OFF}} = \int_{t_3}^{t_3+\Delta t} P_{\mathrm{OFF}}(t) \cdot dt \le E_{\mathrm{OFF\_max}} \end{cases} \tag{7}$$

$$E_{\mathrm{MOV}} = \int_{t_3}^{t_4} U_{\mathrm{MOV}} \cdot I_{\mathrm{MOV}} \cdot dt < E_{\mathrm{MOV\_max}}. \tag{8}$$

Based on the HCB operation process and the motion analysis, the ultrafast MS has been designed with the target of a rated voltage of 750 V and a rated current of 500 A. Considering the actual engineering conditions (including operating temperature and volume), the precharging capacitors are selected as the film capacitors, with a total capacitance of 500 μF and a rated voltage of 500 V. To ensure that the movable contact can reliably keep in the closed position and not be repelled due to the Holm force when carrying the fault current, the closed holding force of two coupling springs is set to approximately 30 N. The minimum distance between the opening Thomson coil and the movable contact is designed to be approximately 2 mm, considering the insulation issues of the primary and secondary circuits.

Based on these given conditions, other significant structural parameters (the number of windings for the opening Thomson coil, the diameter, and the thickness of the movable contact with the integrated metal repulsive disc function) can be simulated using electromagnetic simulation software and the motion simulation software, such as Ansys Maxwell and ADAMS. The electromagnetic force on the movable contact can be extracted from the electromagnetic simulation software, and the displacement of the movable contact can then be obtained from the motion simulation software, considering factors such as electromagnetic force, spring force, and mechanical collisions. Finally, the number of windings for the opening Thomson coil is designed as 52, and the diameter and the thickness of the movable contact are 30 mm and 3 mm, based on the optimized simulation results.

IV. Prototype Development and Experiments

Now, for the classical low-voltage dc system rated at 1500 V ($\pm$750 V), an ultrafast MS with a rated current of 500 A has been developed, as shown in Fig. 8(a). Based on the proposed ultrafast MS and the bidirectional diode-bridge PES, a 750V HCB has also been developed to verify the effectiveness of the novel ultrafast MS solution, as shown in Fig. 8(b). The drive circuit for the ultrafast MS is shown in Fig. 8(c), and the whole size of the ultrafast MS integrating the drive circuit is approximately 260 mm$\times$50 mm$\times$85 mm. The selected parameters of the ultrafast HCB prototype are illustrated in Table I.

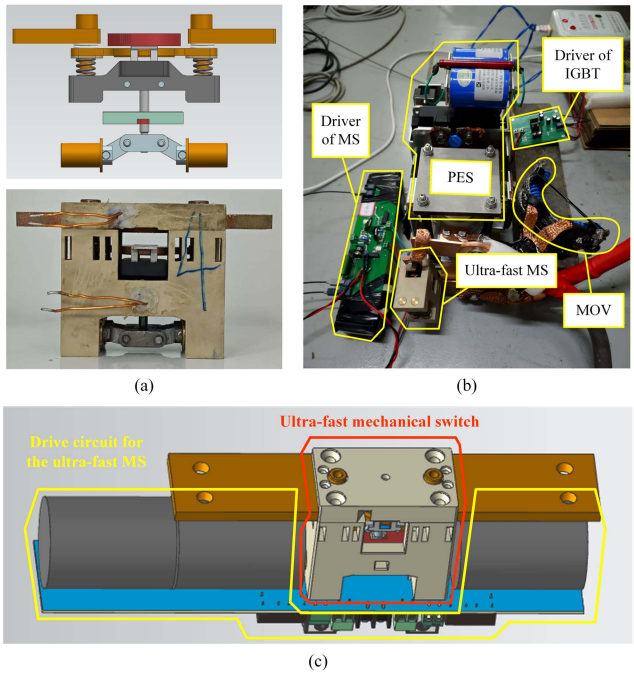

Fig. 8. Developed prototype of the ultrafast MS and the related HCB. (a) 750 V/500 A ultrafast MS. (b) Developed 750 V HCB prototype. (c) Complete ultrafast MS integrating the drive circuit.

TABLE I
PROTOTYPE PARAMETERS

Drive circuit the of proposed ultrafast MS	U_{P} and C_{P}	450 V/500 μF
	L_1 and R_1	30 μH/80 mΩ
	SCR	KY-TYN8012 (1200 V / 80 A)
PES module	IGBT	CRRC-TIM3600E2SM17 (1.7 kV / 3.6 kA) (Clarification: It has a desaturation current greater than 30 kA at a 25 V gate voltage.)
	Diode	CRRC-ZP9 2700-18 (1.8 kV / 2.7 kA)
	Snubber Circuit	R-C-D with R_{S} = 5Ω, C_{S} = 240 μF, and D_{S} of 2 × PERI-MZK400TS120S (1.2 kV / 800 A)
	MOV	750 V @ 1 mA / 1100 V @ 26 kA E_{MOV} > 10 kJ
Drive circuit of the IGBT	V_{GE}	25 V of ON and -10 V of OFF
	C_{GE}	470 nF
	R_{ON}	1.5 Ω
	R_{OFF}	30 Ω

A. Experiments for Ultrafast MS

The mechanical opening separation process of the ultrafast MS is captured through a high-speed camera. The high-speed camera used captures at a rate of 40 μs per frame. Fig. 9(a) and (b) shows the motion trajectories of the movable contact, along

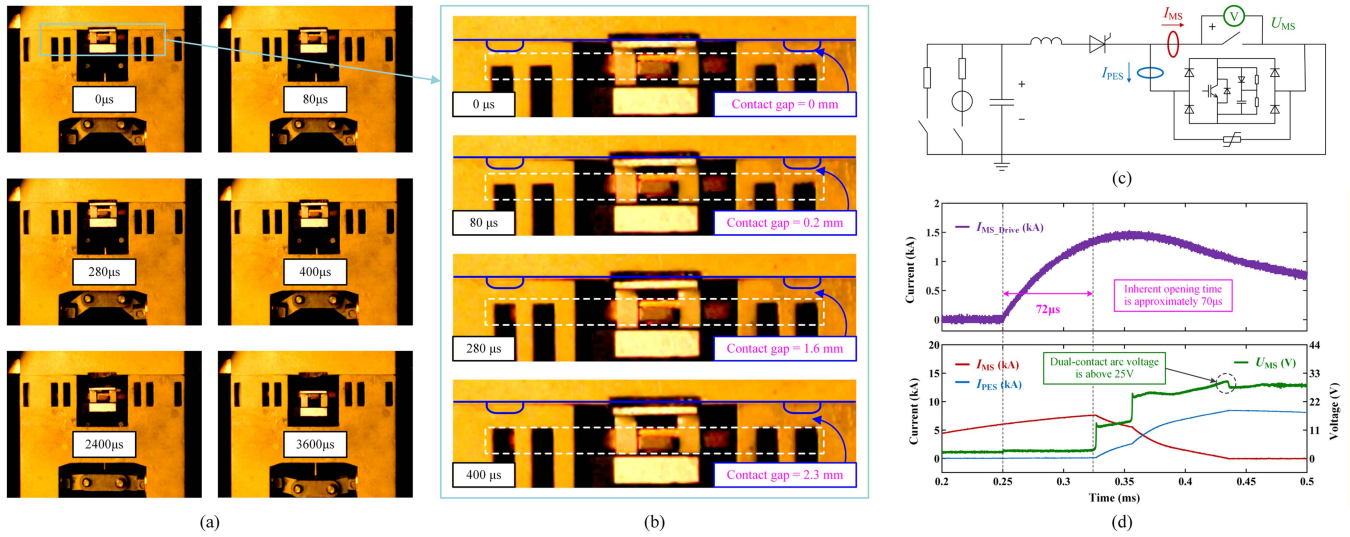

Fig. 9. Experiments for the proposed ultrafast MS. (a) Motion trajectory of the ultrafast MS in opening operation. (b) Distance of the contact gap at different moments. (c) Equivalent testing circuit for DC breaking. (d) Test of the inherent opening time and arc voltage for the ultrafast MS.

with the contact gap at four significant moments. At 0 μs, the MS is triggered. At 80 μs, the movable contact has separated from the stationary contact. Before 320 μs, the movable contact strikes the insulation block and continues to move downward as an integral whole. At the moment the insulation block is struck, the contact gap is sufficient to withstand the 1.5 kV overvoltage caused by the PES's current interruption. At 400 μs, the contact gap has further reached the safe value of 2.3 mm. After 400 μs, the insulation block pulls the bistable holding mechanism downward, reaching a stable opening state in a low-speed mode.

Fig. 9(c) illustrates the classical equivalent testing circuit for dc breaking, which uses a precharged capacitor to discharge the inductor, generating a simulated fault current. The testing circuit is configured with an adjustable inductance of 4–10 μH and a capacitance of 30 mF. Based on the testing circuit, the inherent opening time and the arc voltage of the ultrafast MS are measured, as shown in Fig. 9(d). A simulated fault current is generated prematurely and reaches 5 kA before 0.25 ms. The drive circuit of the ultrafast MS is activated at 0.25 ms, and the movable contact actually separates from the stationary contact after 72 μs. Then, the arc voltage within the two sets of contacts gradually develops and stays above 25 V. With the enhanced dual arc voltage, the current quickly transfers to the PES from the ultrafast MS. Besides, the IGBT turns ON at 0.25 ms and turns OFF after the simulated testing current crosses zero to measure the arc voltage accurately by the low-voltage mode of the differential voltage probe without any risk of high voltage.

B. Experiments for HCB

For the 750 V HCB prototype, as long as a fault current rise rate is within the allowable range, the HCB always interrupts the fault current at a specified 400 μs moment after receiving the opening command. With the current rise rate of 25 A/μs and 50 A/μs, the current interruption experiment results are shown in Fig. 10(a) and (b). For a *di/dt* of 50 A/μs, as shown

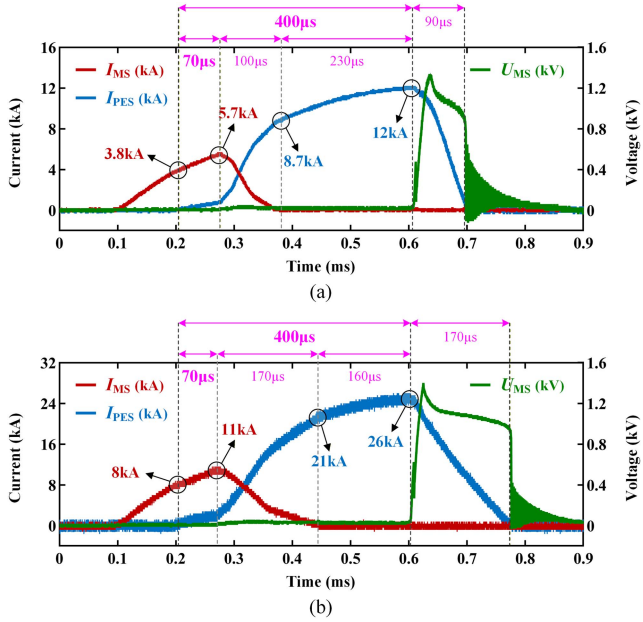

Fig. 10. The experiment result obtained from a 750 V ultra-fast HCB prototype. (a) Testing results of breaking a 12 kA current (with di/dt = 25 A/μs). (b) Testing results of breaking a 26 kA current (with di/dt = 50A /μs).

in Fig. 10(b), the simulated fault started at 0.1 ms. The HCB prototype received the opening command at 0.2 ms. At this moment, the drive circuit of the ultrafast MS discharged the Thomson coil. Although movable and stationary contacts keep closed, a closing resistance is increasing, causing a part of the current to transfer to the PES passively. The real current commutation started at 0.27 ms and ended before 0.44 ms. The IGBT turned OFF a 26 kA current at 0.6 ms. Finally, the MOV limited the subsequent switching overvoltage below 1.5 kV. Besides, as shown in Fig. 10(a), the simulated fault current with a lower *di/dt* (25 A/μs) is also interrupted within 400 μs successfully based on the same operation processes. The experiments verified the

TABLE II
PARAMETERS COMPARISON

Parameters Type		Current interruption time: Inherent opening time	Current interruption time: Arc voltage rise time	Energy dissipation time	Interruption current value and time	Breaking energy	Total size
Air circuit breaker	Eaton's Breaktor	≈1 ms	≈3 ms	<0.1 ms (τ≈0)	25 kA/4 ms	Low	Small
	ABB's Gerapid	≈5 ms	≈3 ms	≈8 ms (di/dt=25 A/μs)	100 kA/8 ms	High	Medium

Parameters Type		Current interruption time: Inherent opening time	Current interruption time: Current commutation time	Current interruption time: Dielectric recovery time	Energy dissipation time	Interruption current value and time	Breaking energy	Total size
Hybrid circuit breaker	HCB solution in [14]	≈0.7 ms	≈1.3 ms	≈1 ms	≈1 ms (di/dt=5 A/μs)	15 kA/3 ms	High	Large
	Proposed ultra-fast HCB	70 μs	170 μs	160 μs	≈0.2 ms (di/dt=50 A/μs)	26 kA/0.4 ms	High	Medium

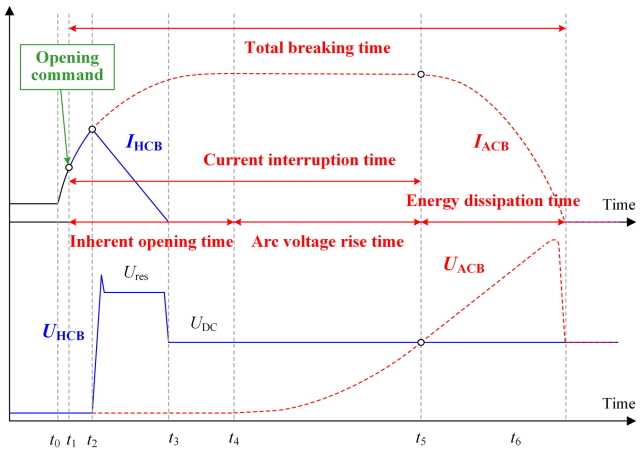

Fig. 11. Definition of the breaking time for DC circuit breakers.

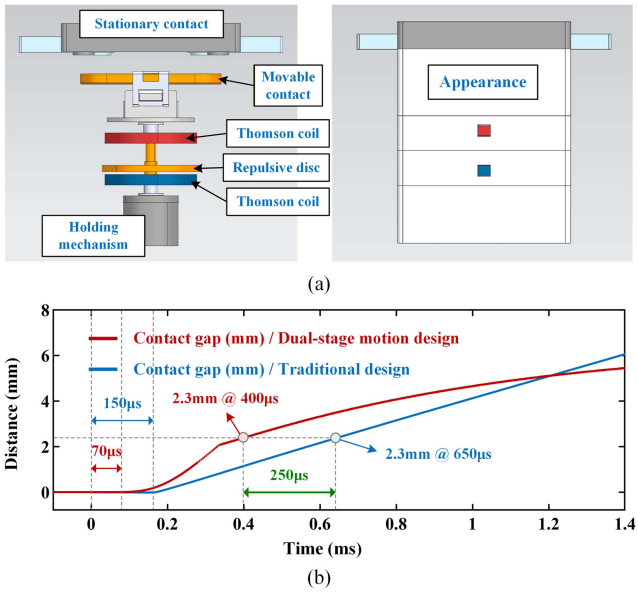

Fig. 12. Comparison with the scaled-down fast MS based on a traditional design. (a) Structure of the scaled-down fast MS. (b) Simulation results.

feasibility of the proposed solution. In engineering, based on the maximum fault current di/dt of different systems, the ultrafast MS can be configured with the PES of various capacities for reduced cost and miniaturized size of the whole HCB.

V. PERFORMANCE COMPARISON

Due to the differences in dc breaking principles between ACB and HCB, it is essential to standardize the definitions of the time intervals corresponding to each stage of dc breaking operation, as shown in Fig. 11, in order to prevent unnecessary confusion. The breaking time for DCCB consists of two parts: the current interruption time and the energy dissipation time. For the ACB, the current interruption time is obviously longer than that of the HCB and can be further divided into two parts: the inherent opening time and the arc voltage rise time.

Finally, the performance and key parameters of the proposed ultrafast HCB solution are compared with those of the existing ACB products and HCB solutions, as much as possible under similar reference conditions. For the ACB, Eaton's Breaktor and ABB's Gerapid dc breaker are compared as existing products, respectively. For the HCB, a similar HCB solution based on the natural commutation principle is selected for the comparison [14]. The comparison results are illustrated in Table II, and the proposed ultrafast HCB has real advantages in operating speed, interrupting capacity, and capacity density.

For a fairer comparison, another fast MS with the same rated parameters of 750 V and 500 A has been designed, as shown in Fig. 12. Compared to the proposed ultrafast MS, this scaled-down fast MS retains the traditional structural design but only eliminates the arc extinguish chamber. Based on the simulation results, the inherent opening time of the fast MS is 150 μs, and it takes 650 μs to achieve a 2.3 mm distance of the contact gap, which is sufficient to withstand the PES's turn-OFF overvoltage. The comparison demonstrates that the dual-stage motion design can improve the contact separation speed due to the lightweight concept. The benefits are unrelated to the voltage level.

VI. CONCLUSION

This letter proposes an ultrafast low-voltage HCB solution based on a novel arc-enhanced lightweight MS. By eliminating the arc extinguishing chamber and utilizing a novel dual-stage

lightweight motion design, the proposed ultrafast MS achieves an extremely fast separation speed. Meanwhile, the structure of double-point contact design enhances the arc voltage, enabling faster current commutation without bulky auxiliary devices. Through the parameter design, a compact 750-V HCB prototype has been developed to verify its feasibility.

REFERENCES

[1] T. Dragičević et al., "DC microgrids—Part II: A review of power architectures, applications, and standardization issues," *IEEE Trans. Power Electron.*, vol. 31, no. 5, pp. 3528–3549, May 2016.

[2] N. Flourentzou, V. G. Agelidis, and G. D. Demetriades, "VSC-based HVDC power transmission systems: An overview," *IEEE Trans. Power Electron.*, vol. 24, no. 3, pp. 592–602, Mar. 2009.

[3] M. K. Bucher and C. M. Franck, "Fault current interruption in multiterminal HVDC networks," *IEEE Trans. Power Del.*, vol. 31, no. 1, pp. 87–95, Feb. 2016.

[4] J. Yang, J. E. Fletcher, and J. O'Reilly, "Short-circuit and ground fault analyses and location in VSC-based DC network cables," *IEEE Trans. Ind. Electron.*, vol. 59, no. 10, pp. 3827–3837, Oct. 2012.

[5] S. Zheng, R. Kheirollahi, J. Pan, L. Xue, J. Wang, and F. Lu, "DC circuit breakers: A technology development status survey," *IEEE Trans. Smart Grid*, vol. 13, no. 5, pp. 3915–3928, Sep. 2022.

[6] R. Ma et al., "Investigation on arc behavior during arc motion in air DC circuit breaker," *IEEE Trans. Plasma Sci.*, vol. 41, no. 9, pp. 2551–2560, Sep. 2013.

[7] W. Wen, J. Fan, B. Li, Q. Sun, J. Song, and M. Popov, "Novel over-current tripping device with multilevel adjustment capability based on magnetic coupling for air circuit breakers in DC traction system," *IEEE Trans. Power Electron.*, vol. 39, no. 10, pp. 12107–12112, Oct. 2024.

[8] R. Rodrigues, Y. Du, A. Antoniazzi, and P. Cairoli, "A review of solid-state circuit breakers," *IEEE Trans. Power Electron.*, vol. 36, no. 1, pp. 364–377, Jan. 2021.

[9] X. Zhang, T. Shan, J. Luo, Y. Zhang, T. Zhan, and L. Qi, "Development of a thyristor-assisted hybrid DC circuit breaker for reduced cost and size," *IEEE Trans. Power Electron.*, vol. 38, no. 9, pp. 10569–10573, Sep. 2023.

[10] X. Zhang et al., "A state-of-the-art 500-kV hybrid circuit breaker for a dc grid: The world's largest capacity high-voltage dc circuit breaker," *IEEE Ind. Electron. Mag.*, vol. 14, no. 2, pp. 15–27, Jun. 2020.

[11] W. Wen et al., "Research on operating mechanism for ultra-fast 40.5-kV vacuum switches," *IEEE Trans. Power Del.*, vol. 30, no. 6, pp. 2553–2560, Dec. 2015.

[12] W. Wen et al., "A novel high-efficient and miniaturized operating method for ultra-fast vacuum switch," *IEEE Trans. Power Electron.*, vol. 39, no. 8, pp. 9518–9525, Aug. 2024.

[13] A. Hassanpoor, J. Häfner, and B. Jacobson, "Technical assessment of load commutation switch in hybrid HVDC breaker," *IEEE Trans. Power Electron.*, vol. 30, no. 10, pp. 5393–5400, Oct. 2015.

[14] Z. Yu, Z. Gan, L. Qu, X. Yan, X. Wang, and Y. Huang, "Natural commutation type hybrid DC circuit breaker based on hybrid mechanical gaps," *IEEE Trans. Power Del.*, vol. 38, no. 3, pp. 1848–1858, Jun. 2023.

[15] J. Wang, G. Liang, X. Zhang, L. Qi, and L. Chen, "An IGBT current boosting method by using ultrahigh driving-voltage in HVdc circuit breaker applications," *IEEE Trans. Power Electron.*, vol. 37, no. 7, pp. 8146–8156, Jul. 2022.

[16] T. Shan, X. Zhang, X. Cao, T. Zhan, and L. Qi, "A cost-effective design of soft turn-off diode-bridge power electronic switch for high-performance hybrid DC circuit breakers," *IEEE Trans. Ind. Electron.*, doi: 10.1109/TIE.2025.3577326.